The Ternary Zintl Phases $K_{4-x}Na_xSi_4$ ($1 \le x \le 2.2$) and K_7NaSi_8 – Synthesis, Crystal Structure, and Solid State NMR Spectroscopic Investigations

Lavinia M. Scherf,[a] Oliver Pecher,[b] Kent J. Griffith,[b] Frank Haarmann,[c,d] Clare P. Grey,[b] and Thomas F. Fässler*[a]

Dedication ((optional))

Abstract: The Zintl phases $K_{4-x}Na_xSi_4$ ($1 \le x \le 2.2$) and K_7NaSi_8 are the first ternary phases in the K-Na-Si system and both contain tetrahedral $[Si_4]^{4-}$ clusters next to a charge-balancing number of K^+ and Na^+ cations. All phases $K_{4-x}Na_xSi_4$ ($1 \le x \le 2.2$) crystallize in a new structure type with space group $P2_1/n$, as determined via single crystal X-ray diffraction of the parent phase K_3NaSi_4. Rietveld refinement of X-ray diffraction data showed that the solid solutions follow Vegard's rule. K_7NaSi_8 can only be synthesized by diffusion controlled reaction of binary precursors and is isostructural to the known $A_7A'T_8$ (A = Na – Cs, A' = Li, Na, T = Si, Ge) phases. A combination of solid-state NMR investigations and QM calculations serves to show the anisotropic chemical bonding behavior of all atoms in K_7NaSi_8 which is additionally compared to the related phases A_7NaSi_8 (A = Rb, Cs).

Introduction

Most binary alkali metal silicides and germanides in the phase systems A - T (A = Li – Cs; T = Si, Ge) are typical examples of Zintl phases. These polar intermetallic compounds can be described by a formal electron transfer from the electropositive alkali metal to the more electronegative tetrel (T) atoms. The resulting tetrel anions form substructures that can often be rationalized using the octet or ($8 - N$) rule.[1]

In lithium tetrelides, the Li cations can stabilize a large variety of polyanions of the tetrel elements[2] due to a strong covalent contribution to the Li–T bonds. Such polyanions include three-dimensional substructures in the compounds LiT[3] and two-dimensional slabs of T atoms in Li_7Ge_{12} and Li_3NaSi_6.[4,5] Often, small anionic tetrel clusters are observed such as dumbbells in Li_7T_3[6] and Li_3NaGe_2,[7] and Friauf polyhedra $[Li@Li_4Ge_7]^{12-}$ in $Li_{18}Na_2Ge_{17}$ and Li_7RbGe_8.[8] The latter two Zintl phases also contain tetrahedral $[Ge_4]^{4-}$ clusters. The Li-rich binary tetrelides such as $Li_{17}T_4$, $Li_{4.1}T_4$ and $Li_{15}T_4$ seem to evade compositions such as Li_4T allowing a salt-like and valence electron precise situation.[9]

In contrast, the alkali metals heavier than lithium only form less alkali metal-rich silicides and germanides with binary A_4T_4 (A = Na – Cs)[10,11] being the most alkali metal-rich phases. Aside from clathrate-type phases[12] their anionic substructures comprise only either tetrahedral $[T_4]^{4-}$ or deltahedral $[T_9]^{4-}$ clusters or both. These clusters are separated and balanced by an appropriate number of alkali metal cations, resulting in various binary and ternary Zintl phases with differing structure types. Binary phases include A_4T_4 (A = Na – Cs),[10,11] A_4Ge_9 (A = K – Cs)[13] and $A_{12}T_{17}$ (A = Na – K),[14] and the ternary phases A_7NaSi_8 (A = Rb, Cs),[15-18] A_7NaGe_8 (A = K – Cs),[19,20] $Cs_2Na_2Ge_4$[21] and $K_6Rb_6Si_{17}$[22] have also been reported. Additionally, the semiconductor Ba_2Si_4 with slightly distorted $[Si_4]^{4-}$ units[23,24] as well as the metallic Zintl phase Ba_3Si_4 comprising butterfly-like $[Si_4]^{6-}$ anions[25] have been prepared.

Alkali metal silicides and germanides have been proven to be suitable precursors for a broad range of new Si and Ge materials. For example, thermal decomposition of Na_4Si_4 under vacuum yields the guest-free clathrate $\square_{24}Si_{136}$.[26] Guest-free Ge clathrates $\square_{24}Ge_{136}$ can be prepared by oxidation of Na_4Ge_9 in ionic liquids.[27] Oxidation of Li_7Ge_{12} with protic solvents leads to the topochemical formation of *allo*-Ge, a crystalline Ge allotrope.[4,5,28] Amorphous Si is obtained upon both oxidation of Li_3NaSi_6 with protic solvents and extraction of $Li_{15}Si_4$ with liquid ammonia.[29] Using surfactants, elemental nanostructures such as hexagonal mesoporous Ge can be synthesized from K_4Ge_9 and polymeric $^1_\infty[Ge_9]^{2-}$ solutions.[30] Polymethylmethacrylate (PMMA) opals can function as templates for the synthesis of inverse opal structured Ge from solutions of $[Ge_9]^{4-}$ clusters.[31]

In addition, Zintl phases containing tetrahedral $[Si_4]^{4-}$ and $[Ge_4]^{4-}$ anions have been shown to be efficient precursors for nanocrystalline Si and Ge. Kauzlarich et al. have shown that binary Na_4Si_4, K_4Si_4 and Na_4Ge_4 as well as ternary Rb_7NaSi_8 can be reduced to Si and Ge nanoparticles upon reaction with TCl_4 or NH_4Br.[32] Depending on the workup procedure, the particle surfaces can be capped with different functional groups.[33,34] In addition, it was possible to monitor the synthesis of alkyl-capped Si nanoparticles from Na_4Si_4 and $SiCl_4$ via NMR spectrometry.[34] Furthermore, the binary compounds A_4T_4, A_4Ge_9, and $A_{12}T_{17}$ are

[a] L. M. Scherf, Prof. Dr. T. F. Fässler
Department of Chemistry
Technical University of Munich
Lichtenbergstraße 4, 85747 Garching/München (Germany)
E-mail: Thomas.faessler@lrz.tum.de
[b] Dr. O. Pecher, K. J. Griffith, Prof. C. P. Grey
Department of Chemistry
University of Cambridge
Lensfield Road, Cambridge, CB2 1EW (UK)
[c] Dr. F. Haarmann
Institute of Inorganic Chemistry
RWTH Aachen University
Landoltweg 1, 52073 Aachen (Germany)
[d] Dr. F. Haarmann
Max Planck Institute for Chemical Physics of Solids
Nöthnitzer Str. 40, 01187 Dresden (Germany)

Supporting information for this article is given via a link at the end of the document.

frequently used as precursors for the preparation and modification of Zintl clusters in solution.[35,36]

The combined application of nuclear magnetic resonance (NMR) spectroscopy and quantum chemical (QM) calculations allows the chemical bonding in intermetallic phases and the anisotropy of charge distribution to be investigated and rationalized.[37,38] Anisotropy is accessible via the so-called quadrupole coupling, i.e., the interaction of the electric field gradient (EFG) with the nuclear quadrupole moment.[37] Some of us have recently applied this approach to gain insights into the chemical bonding of the Zintl phases A_4Si_4 (A = Na – Cs) and A_7NaSi_8 (A = Rb, Cs), which all contain tetrahedral $[Si_4]^{4-}$ clusters. [15,16,23] In solid solutions $Rb_7NaSi_{8-x}Ge_x$ the presence of mixed $(Si_{4-x}Ge_x)^{4-}$ clusters could be proven using these techniques.[36]

In order to broaden the selection of possible precursors for Zintl ions in solutions and the synthesis of novel materials we have been searching for new alkali metal tetrelides by mixing different alkali metal cations. As seen in the various ternary phases, employing cations of different sizes such as Na and K can stabilize different structure types and polyanions. Herein, we present the synthesis of two new Zintl phases in the $K_{4-x}Na_xSi_4$ system comprising tetrahedral $[Si_4]^{4-}$ clusters: the solid solution $K_{4-x}Na_xSi_4$ ($1 \le x \le 2.2$) and K_7NaSi_8 have been structurally characterized by X-ray diffraction (XRD). Furthermore, solid-state NMR and QM calculations were utilized to gain insights into the chemical bonding of K_7NaSi_8 in a comparative study with A_7NaSi_8 (A = Cs, Rb).

Results and Discussion

The $K_{4-x}Na_xSi_4$ System

Figure 1 shows the different phases identified in the $K_{4-x}Na_xSi_4$ system as part of this study. Prior to this work only the binary phases K_4Si_4 ($P\bar{4}3n$)[11] and Na_4Si_4 ($C2/c$)[39] were known, K_3NaSi_4 and $K_{3.5}Na_{0.5}Si_4$, crystallizing with space group $P2_1/n$ and $Pa\bar{3}$, respectively being identified for the first time. K_4Si_4, $K_{3.5}Na_{0.5}Si_4$ and Na_4Si_4 are stoichiometrically exact phases, whereas solid solutions such as K_3NaSi_4 exist in the range of $1 \le x \le 2.2$. The four phases crystallize in four different structure types and space groups. $K_{3.5}Na_{0.5}Si_4$ is isostructural to the known phases A_7NaSi_8 (A = Rb, Cs),[15,16] K_7LiGe_8,[18] A_7NaGe_8 (A = K – Cs),[19,20] and A_7LiSi_8 (A = K – Cs)[17,18] and will therefore be denoted as K_7NaSi_8 from now on.

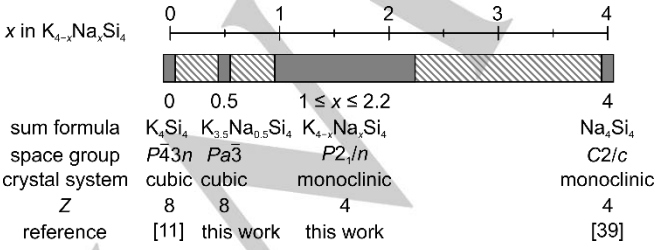

Figure 1. Zintl phases in the $K_{4-x}Na_xSi_4$ system and their structure types. Grey blocks symbolize single-phase regions and shaded areas are two-phase regions.

Synthesis of K_3NaSi_4

In an initial experiment aimed at the synthesis of "K_3NaSi_9" the novel ternary Zintl phase K_3NaSi_4 was obtained in addition to unreacted Si. Nearly phase-pure K_3NaSi_4 can be synthesized from the binary precursors K_4Si_4 and Na_4Si_4 according to equation (1) or from a stoichiometric mixture of the pure elements at 600 °C in sealed Nb ampoules. The latter synthesis method yielded single crystals suitable for X-ray structure analysis.

$$3\ K_4Si_4 + Na_4Si_4 \rightarrow 4\ K_3NaSi_4 \qquad (1)$$

K_3NaSi_4 crystallizes in the monoclinic space group $P2_1/n$ (Table 1) in a new structure type comprising three K, one Na, and four Si positions (all Wyckoff position 4*e*, Figure 2a). The Si atoms form a slightly distorted $[Si_4]^{4-}$ tetrahedron with typical Si distances (2.38–2.46 Å) and angles (58.6–61.6°). Its coordination sphere (Figure 2b) consists of three face-capping η^3-K ligands, two η^2-Na and η^2-K ligands each and eight terminal ligands (seven K and one Na). The corresponding K-Si and Na-Si distances of 3.30–3.86 Å and 2.98–3.11 Å, respectively (s. Table S2), are comparable to those in K_4Si_4 and Na_4Si_4.[11,39]

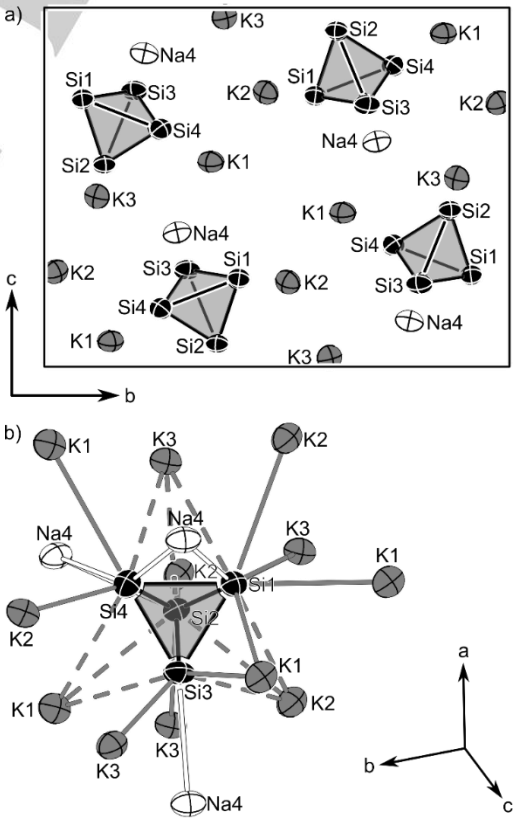

Figure 2. a) Projection of the unit cell of K_3NaSi_4 onto the *bc*-plane; b) coordination sphere of $[Si_4]^{4-}$ tetrahedra. Anisotropic displacement parameters are shown with 90 % probability at 100 K.

Table 1. Crystal structure data for K_3NaSi_4.

	K_3NaSi_4
Formula	K_3NaSi_4
M_r, g mol^{-1}	252.65
Cryst. size, mm^3	0.31 × 0.20 × 0.14
Crystal shape	block
Crystal system	monoclinic
Space group	$P2_1/n$ (No. 14)
a, Å	6.6791(5)
b, Å	13.685(1)
c, Å	10.7427(9)
β, °	100.667(4)
V, Å^3	965.0(1)
Z	4
D_{calcd}, g cm^{-3}	1.739
μ(MoK_α), cm^{-1}	1.868
F(000), e	496
Θ range, °	2.44–31.62
hkl range	±8, ±16, ±12
Refl. measured	22693
Refl. unique	1753
R_{int}	0.0526
Param. refined	73
Restraints	0
$R(F)/wR(F^2)$[a] [$I > 2\sigma(I)$]	0.0346 / 0.0920
$R(F)/wR(F^2)$[a] (all reflections)	0.0395 / 0.0961
GoF (F^2)[b]	1.244
$\Delta\rho_{fin}$ (max/min), e Å^{-3}	0.443 / −0.448

[a] $R(F) = \sum||F_o| - |F_c|| / \sum|F_o|$, $wR(F^2) = [\sum w(F_o^2 - F_c^2)^2 / \sum w(F_o^2)^2]^{1/2}$, $w = [\sigma^2(F_o^2) + (0.0318P)^2 + 3.4316]^{-1}$ mit $P = (F_o^2 + 2F_c^2) / 3$; [b] $GoF = [\sum w(F_o^2 - F_c^2)^2 / (n_{obs} - n_{param})]^{1/2}$.

Solid solutions $K_{4-x}Na_xSi_4$ ($1 \le x \le 2.2$)

Further experiments in the K-Na-Si system revealed that K_3NaSi_4 is not a stoichiometrically exact phase but rather a solid solution $K_{4-x}Na_xSi_4$ with $1 \le x \le 2.2$ in which the K cations can be partially substituted by more Na.[40]

The solid solution range was obtained from Rietveld analysis (Table S4) of powder X-ray diffraction patterns that were obtained from a series of products from the synthesis route by mixing binary phases (equation 2). Rietveld refined diffraction patterns of $K_{4-x}Na_xSi_4$ with $1 \le x \le 2.2$ are shown in Figure S2-S5 in the Supporting Information.

$$(4 - x)\ K_4Si_4 + x\ Na_4Si_4 \rightarrow 4\ K_{4-x}Na_xSi_4 \quad x = 1, 1.5, 2, 2.5 \qquad (2)$$

Whereas higher Na contents in the initial reaction mixture lead to the appearance of Na_4Si_4 as a side phase, reaction mixtures with Na contents of $x \le 1$ contain the new ternary phase K_7NaSi_8 which will be discussed in a later section.

In accordance with Vegard's rule[41] the unit cell volume of the solid solutions $K_{4-x}Na_xSi_4$ in $P2_1/n$ decreases approximately linearly with increasing Na content (Figure 3a). As expected, these unit cell volumes are between those of K_4Si_4 and $K_{3.5}Na_{0.5}Si_4$ on one side and Na_4Si_4 on the other. The cell parameters *a*, *b* and *c* for the monoclinic solid solutions ($1 \le x \le 2.2$) also change linearly but not uniformly (Figure 3b): while *a* decreases slightly, a significant decrease of *b* and an increase of *c* occurs with increasing Na amounts.

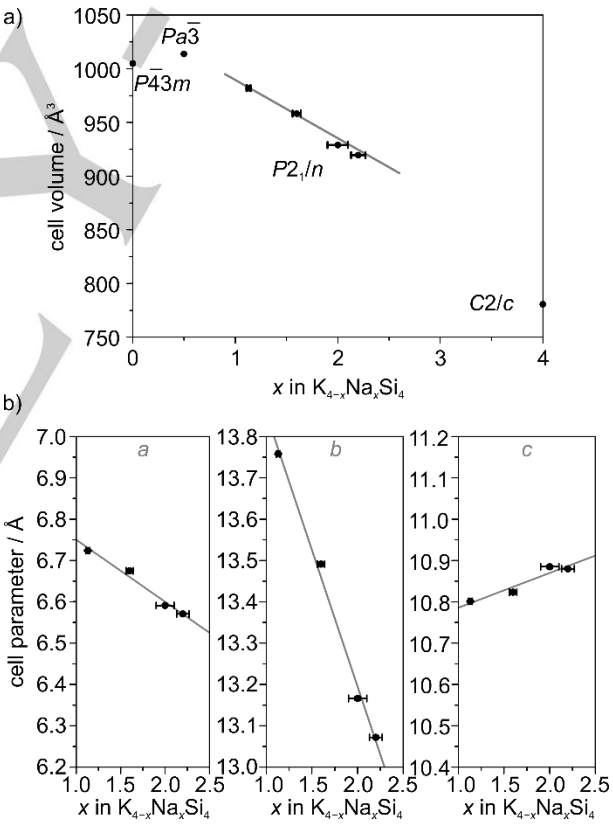

Figure 3. a) Cell volumes of all $K_{4-x}Na_xSi_4$ phases normalized to $Z = 4$; b) Vegard plots[41] illustrating the linear change of cell parameters in space group $P2_1/n$ with increasing Na content in solid solutions $K_{4-x}Na_xSi_4$ ($1 \le x \le 2.2$; alkali metal ratios *x* from Rietveld refinement).Vertical error bars are too small to visible.

These different changes in cell parameters appear reasonable when taking into account the non-random substitution behavior of Na in the $P2_1/n$ solid solutions (Table 2): The crystallographic

positions K1 and Na4 are exclusively occupied by K and Na, respectively. K2 and K3 can however be substituted by Na, but substitution of K3 is clearly preferred up to full Na occupancy. In contrast, K2 is only partially substituted by Na with a maximum

Table 2. Site occupancy factors (s. o. f.) of the four alkali metal positions K/Na1–K/Na4 in solid solutions $K_{4-x}Na_xSi_4$ in space group $P2_1/n$ (x from Rietveld refinement).

x in $K_{4-x}Na_xSi_4$	1.13(2)	1.60(4)	2.0(1)	2.20(7)
s.o.f. K1	1	1	1	1
s.o.f. Na1	0	0	0	0
s.o.f. K2	1	0.85(2)	0.87(6)	0.78(4)
s.o.f. Na2	0	0.15	0.13	0.22
s.o.f. K3	0.87(2)	0.55(2)	0.09(5)	0.02(3)
s.o.f. Na3	0.13	0.45	0.91	0.98
s.o.f. K4	0	0	0	0
s.o.f. Na4	1	1	1	1

Na content of 0.22(4) on this position.

This substitution behavior can be rationalized by a closer inspection of the coordination spheres around the different alkali metal sites in K_3NaSi_4 (Figure S1). The first coordination spheres contain 5–7 Si atoms with interatomic distances of up to 3.856(2) Å (all *A*-Si distances are given in Table S2). A second coordination sphere is clearly separated with *A*-Si distances starting from 4.034(2) Å. As a measure for the available space of the different alkali metal sites, we used average *A*-Si distances. Whereas atom K1 has the largest average distance of 3.603(1) Å to Si atoms, the K2 and K3 sites are significantly smaller with average K-Si distances of 3.475(1) Å and 3.468(1) Å, respectively. The average Na4-Si distance of 3.050(2) Å is again much smaller as it is expected for the smaller alkali metal cation. Therefore, the largest alkali metal site K1 can only stabilize K atoms, whereas K/Na mixing can occur on the smaller K2 and K3 sites. Concurrently, the average *A*-Si distances for K2 and K3 decrease significantly with increasing Na content (Table S3).

Synthesis of K_7NaSi_8

Experiments aimed at the synthesis of Na-poor phases $K_{4-x}Na_xSi_4$ with $x \leq 1$ always yielded mixtures of K_3NaSi_4 and K-richer side phases. However, the identity of the side product phases depends on the method of synthesis. While all high-temperature syntheses and those starting from the elements simply yielded binary K_4Si_4, a different side phase was obtained via the binary reactants route. Using Rietveld refinement this side phase could be identified as K_7NaSi_8. Purer samples were obtained in a reaction from a stoichiometric mixture of the binary reactants K_4Si_4 and Na_4Si_4 (equation 3) as described for Rb_7NaSi_8 and Cs_7NaSi_8,[15,16,42] allowing reliable characterization by Rietveld refinement (Tables 3 and S4).

$$7\ K_4Si_4 + Na_4Si_4 \rightarrow 4\ K_7NaSi_8 \qquad (3)$$

As mentioned earlier, K_7NaSi_8 is isostructural to the known $A_7A'T_8$ phases. Its bright red color is typical for the silicides $A_7A'Si_8$ which, in contrast to the black $A_7A'Ge_8$ phases, have been described as red and transparent.[18] K_7NaSi_8 crystallizes in the cubic space group $Pa\bar{3}$ with a = 12.6563(7) Å which is similar to the cell parameters of cubic K_4Si_4 (a = 12.62 Å, $P\bar{4}3n$).[11] Although the cell parameters of the two cubic phases are so close to each other, they can be clearly distinguished by Rietveld refinement (Figure S6). The Zintl phase comprises tetrahedral $[Si_4]^{4-}$ units which are connected to dimers via η^3-capping Na cations (Figure 4a,b). η^3-Coordination of the tetrahedron yields a K_3NaSi_4 heterocubane in which each Si atom is further coordinated by three terminal K atoms (Figure 4c).

Table 3. Crystallographic data of K_7NaSi_8 obtained from powder diffraction data via Rietveld refinement, adapted from K_7LiSi_8.[17]

	K_7NaSi_8[a]
T / K	293 K
M_r / g mol^{-1}	521.4
Powder color	Grey
Crystal system	Cubic
Space group	$Pa\bar{3}$ (No. 205)
Lattice parameters	
a / Å	12.6563(7)
V / Å^3	2027.3(2)
Z	4
$\rho_{calc.}$ / g cm^{-3}	1.7082
μ / mm^{-1}	18.308
Θ range / °	5.00–89.76
R [I > 3σ(I)]	0.0307
wR [I > 3σ(I)]	0.0317
R (all)	0.0364
wR (all)	0.0324
Goodness of fit	1.38

[a] Sample contains 29.2(5) % K_4Si_4. Slight traces of $K_{4-x}Na_xSi_4$ ($x \approx 1$) could not be quantified.

The Si-Si distances in the slightly distorted tetrahedra are in the range of 2.38–2.48 Å with the longest bonds surrounding the triangular face capped by Na. The Na-Si distance of 2.919(5) Å is in the same range as those in A_7NaSi_8 (A = Rb, Cs).[15,16] K1-Si distances are also typical and in the range of 3.36–3.69 Å, whereas K2 is very distant from its six neighboring Si atoms at 3.905(4) Å. Previous studies have shown that the alkali metal cation in this large cavity can be substituted by larger alkali metals, resulting in the quaternary $AA_6'A''T_8$ aristotype. One such quaternary example is CsK_6NaSi_8[18] which is closely related to the phase described here. The substitution of the K2 position by the larger Cs atom also seems to stabilize the

quaternary phase. Attempts to synthesize K_7NaSi_8 directly from the elements only yielded mixtures of K_4Si_4 and K_3NaSi_4. Thus, K_7NaSi_8 is only accessible from binary starting materials in a diffusion-controlled solid state reaction, whereas CsK_6NaSi_8 is readily available from a stoichiometric melt of the constituent elements.

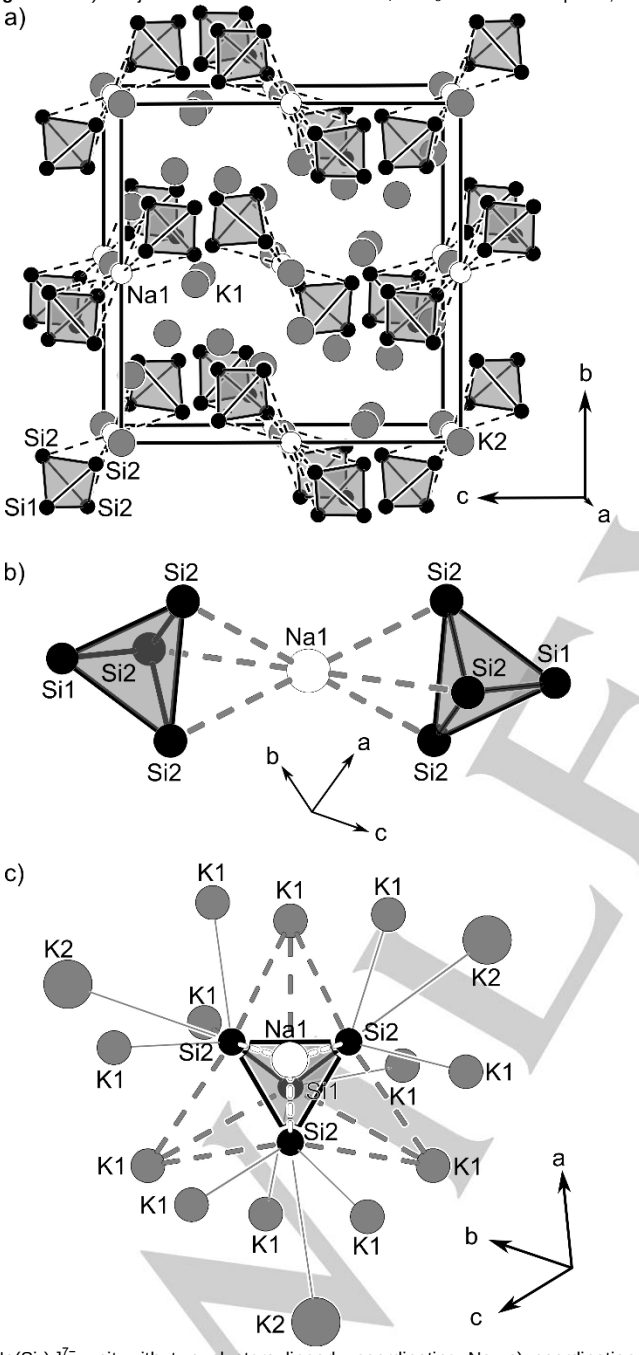

Figure 4. a) Projection of the unit cell of K_7NaSi_8 onto the *bc*-plane; b) $[Na(Si_4)_2]^{7-}$ unit with two clusters linearly coordinating Na; c) coordination sphere of $[Si_4]^{4-}$ tetrahedra. Isotropic displacement parameters are shown with 70 % probability at 293 K. K atoms are shown in grey, Na atoms in white, and Si atoms in black.

Solid-state NMR and QM calculations on K_7NaSi_8

In agreement with the Rietveld refinement, solid-state NMR investigations on a K_7NaSi_8 sample show that this phase is the majority phase comprising one Na and two Si signals at 91.0, -369.7, and -357.2 ppm from the respective crystallographic Na1, Si1, and Si2 positions (Figures 4 and 5, Tables 4 and 5). While second order quadrupole coupling results in broad ^{23}Na NMR MAS and static signal line shapes, comparably high-resolution ^{29}Si NMR signals are visible for the anions (Figure 5). Additional signals and line shape features are due to minority phases of K_3NaSi_4, Na_4Si_4, K_4Si_4, and Na metal (Figure 5, Figures S7–S9).[43] The assignment of the ^{23}Na metal signal is straightforward due to the Knight shifted resonance from the metal at 1120 ppm (Figure S7, Table 5). An unambiguous assignment of all other impurity signals is possible through fits of the NMR line shapes under consideration of NMR coupling parameters derived from QM calculations as starting values (Figure 5, Tables 4 and 5), in which the calculations are based on both the known crystal structures for the binary precursor phases as well as the ones for K_3NaSi_4 and K_7NaSi_8 (Table 1, Tables 3–5, Experimental Section). The parameters derived from NMR and calculations show a reasonable agreement within the experimental error and support the application of NMR spectroscopy in combination with theory to gain insights into the materials on the local atomic scale even for these multi-phase samples.

Interestingly, no ^{29}Si NMR signals of Na_4Si_4 (Si1 and Si2) and K_3NaSi_4 (Si1-Si4) are detected in the measurements although these minority phases are visible in ^{23}Na NMR (Figure 5). Presumably, this is due to the very low amount of these phases within the investigated K_7NaSi_8 sample, which is furthermore in agreement with the 7:1 ratio for the binary precursor phases (Equation 3). Calculations show that the K_3NaSi_4 ^{29}Si shifts span a range of −366.4 to −316.9 ppm for Si1–Si4 and lie in the same frequency range of the K_4Si_4 and K_7NaSi_8 signals, suggesting that our inability to detect the K_3NaSi_4 resonances is either a signal-to-noise ratio or possibly a relaxation issue, rather than our inability to locate the resonance due to the choice of an inappropriate frequency offset.

We now focus on a discussion of the NMR parameters for K_7NaSi_8, which all have been derived by the combined application of solid-state NMR experiment and QM calculations, enabling a discussion of chemical bonding within the series A_7NaSi_8 with A = K, Rb,[15] and Cs[16] (Table S7). With increasing alkali metal atomic number an increase of the ^{29}Si shift is seen for Si1 and Si2 with the same trend of δ_{iso}(Si2) > δ_{iso}(Si1) for all three phases (Table S7, Figure S10). This tendency is in agreement with the order of the signal shifts in A_4Si_4 (A = Na, K,

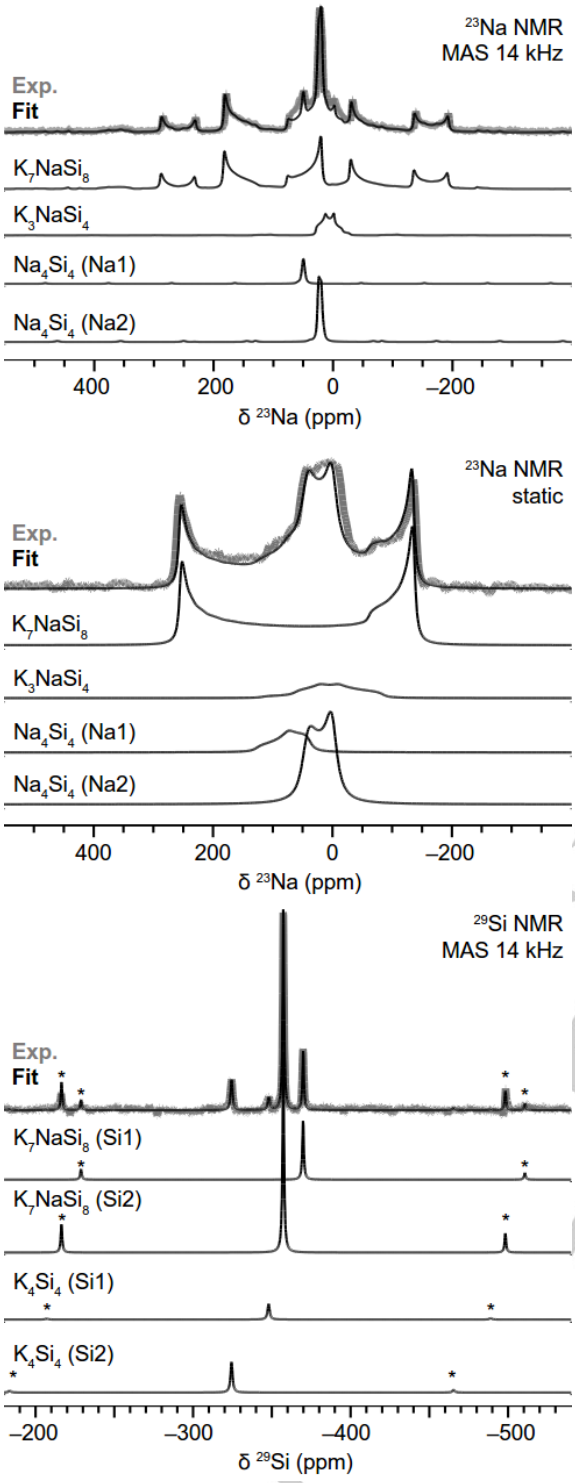

Figure 5. (a) ^{23}Na MAS, (b) ^{23}Na static, and (c) ^{29}Si MAS NMR spectra of K_7NaSi_8. MAS speeds of 14 kHz have been applied; rotational sidebands are marked by asterisks. Experimental data in thick gray, the line shape fit and its contributions in black lines. Signal contributions from different phases are highlighted and labelled in the figure.

Rb, and Cs).[23] The chemical shift anisotropy (CSA, δ_{aniso}) values for Si1 and Si2 in K_7NaSi_8 are identical with the ones for Rb_7NaSi_8 in which the Si1 is smaller and Si2 is larger than for Cs_7NaSi_8 (Table S7, Figure S10). The asymmetry parameters for both Si environments and all three phases are in agreement with the site symmetry and thus zero for Si1 and unequal to zero for Si2 (Table S8).

The isotropic ^{23}Na shift continuously decreases from K_7NaSi_8 to Rb_7NaSi_8 and Cs_7NaSi_8. On the other hand, the CSA values for Na are identical, the asymmetry parameters of zero indicating no difference in the anisotropies for the chemical shift in all three compounds (Table S7, Figure S10). The Na atoms in A_7NaSi_8 (A = K, Rb, and Cs) possess a negative value of the EFG's main component V_{ZZ} which reveals a prolate charge distribution around the nuclei with the largest principal axis along the three-fold axis.

The $|V_{ZZ}|$ values slightly decrease within the series of A = K, Rb, and Cs, which indicates a less pronounced anisotropy of charge distribution around the Na atoms with increasing atomic number and radius of the alkali metal ion (Table S7, Figure S10). Interestingly, this finding is opposite to the slight increase of the interatomic Na—Si2 distance of 2.92(1), 2.94(1), and 2.97(1) Å for A = K, Rb,[15] and Cs,[16] respectively. This indicates that the dimeric linear $[Na(Si_4)_2]^{7-}$ arrangement in A_7NaSi_8 is quite rigid with respect to the alkali metal (Figure 4b). Further support is given by the minor changes of the alkali metal bonding situation (see below). Furthermore, a similar structural motif has been observed in the isotypic A_7NaGe_8 compounds.[19,20]

The difference between the *A*1 and *A*2 isotropic shifts is 81, 177, and 308 ppm for *A* = K, Rb, and Cs, respectively, and shows a continuous increase. The CSA for *A*1 ($\eta_\delta \neq 0$) decreases while the values slightly increase for *A*2 ($\eta_\delta = 0$). More significant differences are visible by comparing the sign and value of V_{ZZ} as a measure of the anisotropy of charge distribution, which is oblate for *A*1 ($\eta_Q \neq 0$) and prolate for *A*2 ($\eta_Q = 0$). The $|V_{ZZ}|$ values increase for both environments with increasing alkali metal radius,
in which $|V_{ZZ}|(A1) > |V_{ZZ}|(A2)$. The $|V_{ZZ}|(A1)/|V_{ZZ}|(A2)$ ratios of 2.9, 2.5, and 2.5 for *A* = K, Rb, and Cs, respectively, indicate similar bonding situations for the alkali metals in A_7NaSi_8 (*A* = K, Rb, and Cs). Nevertheless, the significant difference and increase in the absolute values of $|V_{ZZ}|$ for both sites while comparing K, Rb, and Cs obviously reveals larger anisotropies of charge distribution with increasing alkali metal atomic number and radii. This is in agreement with the higher polarizability of the cations.

Table 5. ^{23}Na NMR coupling parameters derived by NMR signal line shape analysis (exp.) and QM calculations (calc.). The sign of C_Q is provided by the calculations only. Minority and majority phases are indicated by Min. and Maj., respectively.

Atom		δ_{iso} / ppm	δ_{aniso} / ppm	η_δ	C_Q / MHz	η_Q
K_7NaSi_8 (Maj.)						
Na	exp.	91.0	-150.0	0	5.80	0
	calc.	91.7	-167.6	0	-5.60	0
Na_4Si_4 (Min.)						
Na1	exp.	52.3	31.0	0.60	1.26	0.93
	calc.[23]	62.3	31.0	0.60	1.26	0.93
Na2	exp.	26.7	-31.0	0.86	1.90	0.26
	calc.[23]	43.9	-31.0	0.86	2.38	0.26
K_3NaSi_4 (Min.)						
Na	exp.	29.7	-55.0	0.5	4.00	0.5
	calc.	40.0	-51.4	0.49	3.65	0.78
Na metal (Min.)						
Na	exp.[44]	1120	-	-	-	-

Conclusions

During the search for suitable precursors for Zintl ions in solution and nanoparticular material via the mixed cation approach, we have discovered two new Zintl phases containing silicide tetrahedra $[Si_4]^{4-}$. K_3NaSi_4 crystallizes in a new structure type comprising isolated tetrahedra and forms solid solutions $K_{4-x}Na_xSi_4$ with $1 \leq x \leq 2.2$ which obey Vegard's rule. K_7NaSi_8 is isostructural to A_7NaSi_8 (*A* = Rb, Cs) and can only be synthesized by a diffusion controlled reaction of the binary starting materials. A combined application of solid-state NMR investigations and QM calculations reveals anisotropic chemical bonding for all the atoms in A_7NaSi_8 with *A* = K, Rb, and Cs. With increasing atomic numbers and polarizability of the alkali metal the anisotropies of charge distribution significantly increase. A comparably slight decrease is found for the Na atoms. This indicates that the dimeric linear $[Na(Si_4)]^{7-}$ structural motif in A_7NaSi_8 is a quite rigid atomic arrangement. Hence, further studies on similar materials, e.g. the isotypic Ge compounds, are envisioned.

Table 4. ^{29}Si NMR coupling parameters derived by NMR signal line shape analysis (exp.) and QM calculations (calc.). Minority and majority phases are indicated by Min. and Maj., respectively.

Atom		δ_{iso} / ppm	δ_{aniso} / ppm	η_δ	Int.
K_7NaSi_8 (Maj.)					
Si1	exp.	-369.7	150.0	0.00	1.0
	calc.	-353.6	160.1	0.00	1
Si2	exp.	-357.2	150.0	0.00	3.4
	calc.	-343.9	161.8	0.26	3
K_4Si_4 (Min.)					
Si1	exp.	-348.0	150.0	0.00	1.0
	calc.[23]	-339.0	149.3	0.00	1
Si2	exp.	-324.2	153.0	0.00	2.4
	calc.[23]	-313.4	152.9	0.06	3
K_3NaSi_4 (Min.)					
Si1	calc.	-366.4	157.3	0.10	1
Si2	calc.	-333.9	176.8	0.11	1
Si3	calc.	-316.9	133.1	0.21	1
Si4	calc.	-325.5	142.0	0.22	1

Experimental Section

All steps of synthesis and sample preparation were performed inside an Ar-filled glovebox (MBraun, H_2O level < 0.1 ppm, O_2 level < 0.1 ppm). Li rods (99 %, Rockwood-Li), Na pieces (99 %, Chempur) and K (98%, Merck) pieces were freed from oxidic layers before use. Ge (99.999 %, Evochem) and Si pieces (99.99 %) were ground to powder before use.

Synthesis of K_4Si_4, Na_4Si_4

K_4Si_4 and Na_4Si_4 were synthesized from stoichiometric amounts of the elements with a total mass of 2 g in tantalum ampules. The ampules were sealed and placed inside silica reaction containers which were then evacuated. The reaction mixtures were heated up to 500 °C at 5 °C min^{-1}. After one hour of pre-dwelling the ampules were further heated to 600 °C at 5 °C min^{-1} at which temperature dwelling was allowed for 30 h, followed by cooling at 5 °C min^{-1}.

$K_{4-x}Na_xSi_4$ ($1 \leq x \leq 2.2$)

Solid solutions $K_{4-x}Na_xSi_4$ were synthesized from stoichiometric amounts (x = 1, 1.5, 2, 2.5) of K_4Si_4 and Na_4Si_4 with a total mass of 200–250 mg. The starting materials were thoroughly mixed by grinding in an agate mortar and subsequently pressed into pellets (diameter 6 mm). The

pellets were then sealed inside tantalum ampules which were treated as described above. The reaction mixture was heated to 450 °C at 5 °C min^{-1} and dwelled for 7 days. Finally, the samples were cooled to room temperature at 0.1 °C min^{-1}. Alternatively, K_3NaSi_4 was prepared directly from stoichiometric amounts of the elements with a total mass of 500 g in tantalum ampoules using the same heating sequence as for K_4Si_4 and Na_4Si_4.

K_7NaSi_8

K_7NaSi_8 was synthesized from stoichiometric amounts of K_4Si_4 and Na_4Si_4 with a total mass of 500 mg. The starting materials were thoroughly mixed by grinding in an agate mortar and subsequently pressed into pellets (diameter 6 mm). The pellets were then sealed inside tantalum ampules which were treated as described above. The reaction mixture was heated to 450 °C at 5 °C min^{-1} and dwelled for 7 days. Finally, the samples were cooled to room temperature at 0.1 °C min^{-1}.

X-ray structure determination

Crystals of K_3NaSi_4 were sealed in 0.3 mm glass capillaries. Intensity data were collected at 100(2) K using a Bruker AXS X-ray diffractometer equipped with a CCD detector (APEX II, *κ*-CCD), a rotating anode FR591 with Mo K_α radiation (λ = 0.71073 Å), and a MONTEL optic monochromator. Data collection was controlled with the Bruker APEX software package.[45] Integration, data reduction, and multi-scan absorption correction were performed with the SAINT[46] and SADABS[47] packages. The structure was solved with direct methods (SHELXS-2014) and refined with full-matrix least squares on F^2 (SHELXL_2014).[48] Details of the single-crystal data collection and refinement are given in Table 1. Further details of the crystal structure investigation may be obtained from Fachinformationszentrum Karlsruhe, 76344 Eggenstein-Leopoldshafen, Germany (fax: +49-7247-808-666; e-mail: crysdata@fiz-karlsruhe.de, http://www.fiz-informationsdienste.de/en/DB/icsd/depot_anforderung.html) on quoting the deposition number CSD-431197.

Powder X-ray diffraction analysis

All PXRD patterns recorded using a Stoe STADI P diffractometer equipped with a Ge(111) monochromator for Cu K_α radiation (λ = 1.54056 Å) and a Dectris MYTHEN DCS 1K solid-state detector. Samples were prepared by grinding in an agate mortar and then filled into 0.3 mm glass capillaries inside the glovebox which were then sealed. All measured diffraction patterns were angle-corrected with an external *α*-Si standard.

Rietveld refinement

Rietveld refinements were performed using Jana2006.[49] The crystal structures of K_3NaSi_4 and K_7LiSi_8[17] were used as initial structural models. All cell parameters and atom positions as well as site occupancies for mixed positions were refined with the sum of mixed site occupancies set to 1. Isotropic displacement parameters were refined whenever possible.

Solid-state NMR spectroscopy

Static and magic angle spinning (MAS) NMR experiments were performed on a powder sample of K_7NaSi_8 as well as a K_4Si_4 reference sample with a Bruker Avance III console on a 11.7 T magnet. The respective resonance frequencies of ^{29}Si and ^{23}Na are 99.3 and 132.3 MHz, respectively. The signals were acquired using a Bruker 4.0 mm triple resonance probehead with 4.0 mm ZrO_2 rotors at MAS frequencies of 7.5, 12.5, and 14.0 kHz. The ^{29}Si and ^{23}Na NMR shifts are referenced to TMS and NaCl, respectively.[50] A one-pulse sequence with hard pulses of 1.30 μs duration, approximately corresponding to 30° pulses, and a recycle delay of 170 s was used for the ^{29}Si NMR measurements. ^{23}Na NMR signals were acquired with hard pulses of 1.40 μs duration and a recycle delay of 10 s in MAS frequency synchronized Hahn-echo pulse sequences and by applying an interpulse delay of 60 μs for static measurements, respectively. All sample handling was done in an MBraun Argon glovebox with O_2 and H_2O levels < 0.1 ppm to prevent the samples from reacting with moisture and/or air. The powder samples were mixed with vacuum-dried GeO_2 in a 4:1 ratio and pressed into the ZrO_2 rotor. The mixture was topped with a thin layer of pure GeO_2 as well as a Teflon tape seal before closing the rotor with the cap. NMR raw data handling and signal line shape analysis was done using Bruker Topspin (version 2.1) and its implemented SOLA program. We refer to $\delta_{iso} = (\delta_{XX}+\delta_{YY}+\delta_{ZZ})/3$, $\delta_{aniso} = (\delta_{ZZ}-\delta_{iso})$ and $\eta_\delta = (\delta_{YY}-\delta_{XX})/\delta_{aniso}$ for the isotropic chemical shift, the chemical shift anisotropy and the asymmetry parameter of the chemical shielding, respectively.[16] The order of the principal axes of the shielding tensor is defined by $|\delta_{ZZ}-\delta_{iso}| \geq |\delta_{XX}-\delta_{iso}| \geq |\delta_{YY}-\delta_{iso}|$ resulting in $0 \leq \eta_\delta \leq 1$. The quadrupole coupling constant is defined as $C_Q = (V_{ZZ}\cdot e\cdot Q)/h$ with V_{ZZ} as the main component of the electric field gradient (EFG), the elementary charge e, the quadrupole moments Q (5.85, 13.35, and -0.343 fm^2 for ^{39}K, ^{87}Rb, and ^{133}Cs, respectively)[50] as well as Planck's constant h.[16,37] The asymmetry parameter of the quadrupole coupling is defined as $\eta_Q = (V_{YY} - V_{XX})/V_{ZZ}$ with $|V_{ZZ}| \geq |V_{XX}| \geq |V_{YY}|$ and $0 \leq \eta_Q \leq 1$.[16,37] Asymmetry parameters of $\eta = 0$ and $\eta \neq 0$ correspond to axial and non-axial symmetry for the atom under investigation, respectively. Symmetry constraints for the NMR coupling parameters/lineshape due to the site symmetries of the atoms in A_7NaSi_8 (A = K, Rb, and Cs) are summarized in Table S8.

QM calculations

QM calculations of NMR parameters[51] were performed in the gauge-including projector augmented wave method (GIPAW) implemented in the periodic density functional theory (DFT) code CASTEP[52]. The gradient-corrected PBE exchange–correlation functional[53] was used for all calculations. Core electrons were described with Vanderbilt ultrasoft pseudopotentials generated "on-the-fly" in CASTEP 8.0. Chemical shift and quadrupole tensor calculations were performed for each compound with a plane wave basis set truncation energy of 800 eV. The Brillouin zone was sampled with a Monkhorst-Pack grid[54] with k-point sampling finer than $2\pi \cdot 0.02$ $Å^{-1}$. Convergence of the basis set energy and k-point sampling were examined and confirmed. In the discussion of experimentally derived and calculated NMR coupling parameters we refer to a good agreement, which can be achieved within the ranges of ± 10 ppm for δ_{iso} and δ_{aniso}, ± 0.1 MHz for C_Q and $\pm 0.1\cdot10^{21}$ Vm^{-2} for V_{ZZ}, respectively, as has recently been discussed for Zintl phases.[16]

Acknowledgements

We gratefully acknowledge fruitful discussions with Dr. Rachel N. Kerber (Cambridge). L.M.S. is grateful for financial support by Fonds der chemischen Industrie and a fellowship from Studienstiftung des deutschen Volkes. This project has in part received funding from the European Union's Horizon 2020 research and innovation program under the Marie Skłodowska-Curie grant agreement No 655444 (O.P.). K.J.G. thanks the Winston Churchill Foundation of the United States and the Herchel Smith Scholarship for financial support.

Keywords: alkali metal • silicon • Zintl phases • NMR spectroscopy • density functional calculations

[1] a) E. Zintl, *Angew. Chem.* **1939**, *52*, 1–6; b) T. F. Fässler, in *Book Series: Structure and Bonding, Vol. 139* (Ed.: D. M. P. Mingos), Springer-Verlag, Heidelberg, **2011**.
[2] R. Nesper, *Prog. Solid State Chem.* **1990**, *20*, 1–45.
[3] a) E. Menges, V. Hopf, H. Schäfer, A. Weiss, *Z. Naturforsch. B* **1969**, *24*, 1351–1352; b) J. Evers, G. Oehlinger, G. Sextl, *Angew. Chem.* **1993**, *105*, 1532-1534; *Angew. Chem. Int. Ed.* **1993**, *32*, 1442–1444.
[4] A. Grüttner, R. Nesper, H. G. von Schnering, *Angew. Chem.* **1982**, *94*, 933; *Angew. Chem. Int. Ed. Engl.* **1982**, *21*, 912–913.
[5] a) F. Kiefer, T. F. Fässler, *Solid State Sci.* **2011**, *13*, 636–640; b) H. G. von Schnering, M. Schwarz, R. Nesper, *J. Less-Common Met.* **1988**, *137*, 297–310.
[6] a) A. Grüttner, R. Nesper, H. G. v. Schnering, *Acta Crystallogr.* **1981**, *A37*, C161; b) H. G. von Schnering, R. Nesper, K.-F. Tebbe, J. Curda, *Z. Metallkd.* **1980**, *71*, 357.
[7] L. M. Scherf, A. J. Karttunen, O. Pecher, P. C. M. M. Magusin, C. P. Grey, T. F. Fässler, *Angew. Chem.* **2016**, *128*, 1087-1091; *Angew. Chem. Int. Ed.* **2016**, *55*, 1075-1079.
[8] a) L. M. Scherf, M. Zeilinger, T. F. Fässler, *Inorg. Chem.* **2014**, *53*, 2096–2101; b) S. Bobev, S. C. Sevov, *Angew. Chem.* **2001**, *113*, 1555-1558; *Angew. Chem. Int. Ed.* **2001**, *40*, 1507–1510.
[9] a) M. Zeilinger, D. Benson, U. Häussermann, T. F. Fässler, *Chem. Mater.* **2013**, *25*, 1960-1967; b) M. Zeilinger, T. F. Fässler, *Dalton Trans.* **2014**, *43*, 14959-14970; c) M. Zeilinger, V. Baran, L. van Wüllen, U. Häussermann, T. F. Fässler, *Chem. Mater.* **2013**, *25*, 4113-4121; d) E. I. Gladyshevskii, P. I. Kripyakevich, *Kristallografiya* **1960**, *5*, 574–576; e) Q. Johnson, G. S. Smith, D. Wood, *Acta Crystallogr.* **1965**, *18*, 131–132; f) M. Zeilinger, I. M. Kurylyshyn, U. Häussermann, T. F. Fässler, *Chem. Mater.* **2013**.
[10] E. Hohmann, *Z. Anorg. Chem.* **1948**, *257*, 113–126.
[11] R. Schäfer, W. Klemm, *Z. Anorg. Allg. Chem.* **1961**, *312*, 214–220.
[12] a) J. S. Kasper, P. Hagenmuller, M. Pouchard, C. Cros, *Science* **1965**, *150*, 1713–1714; b) C. Cros, M. Pouchard, P. Hagenmuller, *J. Solid State Chem.* **1970**, *2*, 570–581; c) S. Bobev, S. C. Sevov, *J. Am. Chem. Soc.* **1999**, *121*, 3795–3796; d) S. Bobev, S. C. Sevov, *J. Solid State Chem.* **2000**, *153*, 92–105.
[13] a) S. Ponou, T. F. Fässler, *Z. Anorg. Allg. Chem.* **2007**, *633*, 393–397; b) V. Queneau, S. C. Sevov, *Angew. Chem.* **1997**, *109*, 1818-1820; *Angew. Chem. Int. Ed. Engl.* **1997**, *36*, 1754-1756.
[14] a) C. Hoch, M. Wendorff, C. Röhr, *J. Alloy. Compd.* **2003**, *361*, 206–221; b) W. Carrillo-Cabrera, R. Cardoso Gil, M. Somer, Ö. Persil, H. G. von Schnering, *Z. Anorg. Allg. Chem.* **2003**, *629*, 601–608.
[15] a) T. Goebel, Y. Prots, A. Ormeci, O. Pecher, F. Haarmann, *Z. Anorg. Allg. Chem.* **2011**, *637*, 1982–1991.
[16] O. Pecher, M. Esters, A. Görne, B. Mausolf, A. Ormeci, F. Haarmann, *Z. Anorg. Allg. Chem.* **2014**, *640*, 2169-2176.
[17] H. G. von Schnering, M. Schwarz, R. Nesper, *Angew. Chem.* **1986**, *98*, 558–559; *Angew. Chem. Int. Ed. Engl.* **1986**, *25*, 566-567.
[18] M. Schwarz, Dissertation, Universität Stuttgart **1987**.
[19] J. Llanos, R. Nesper, H. G. von Schnering, *Angew. Chem.* **1983**, *95*, 1026–1027; *Angew. Chem. Int. Ed. Engl.* **1983**, *22*, 998.
[20] J. Llanos, Dissertation, Universität Stuttgart **1984**.
[21] H. G. von Schnering, J. Llanos, G. Yu, W. Carrillo-Cabrera, E.-M. Peters, K. Peters, R. Nesper, *Z. Kristallogr. NCS* **1998**, *213*, 661.
[22] V. Quéneau, E. Todorov, S. C. Sevov, *J. Am. Chem. Soc.* **1998**, *120*, 3263-3264.
[23] T. Goebel, A. Ormeci, O. Pecher, F. Haarmann, *Z. Anorg. Allg. Chem.* **2012**, *638*, 1437-1445.
[24] T. Goebel, Y. Prots, F. Haarmann, *Z. Kristallogr. NCS* **2009**, *224*, 7-8.
[25] U. Aydemir, A. Ormeci, H. Borrmann, B. Böhme, F. Zürcher, B. Uslu, T. Goebel, W. Schnelle, P. Simon, W. Carrillo-Cabrera, F. Haarmann, M. Baitinger, R. Nesper, H. G. von Schnering, Y. Grin, *Z. Anorg. Allg. Chem.* **2008**, *634*, 1651-1661.
[26] A. Ammar, C. Cros, M. Pouchard, N. Jaussaud, J.-M. Bassat, G. Villeneuve, M. Duttine, M. Ménétrier, E. Reny, *Solid State Sci.* **2004**, *6*, 393–400.
[27] A. M. Guloy, R. Ramlau, Z. Tang, W. Schnelle, M. Baitinger, Y. Grin, *Nature* **2006**, *443*, 320–323.
[28] F. Kiefer, A. J. Karttunen, M. Döblinger, T. F. Fässler, *Chem. Mater.* **2011**, *23*, 4578–4586.
[29] M. Zeilinger, L.-A. Jantke, L. M. Scherf, F. J. Kiefer, G. Neubüser, L. Kienle, A. J. Karttunen, S. Konar, U. Häussermann, T. F. Fässler, *Chem. Mater.* **2014**, *26*, 6603-6612.
[30] a) G. S. Armatas, M. G. Kanatzidis, *Science* **2006**, *313*, 817–820; b) G. S. Armatas, M. G. Kanatzidis, *Adv. Mater.* **2008**, *20*, 546–550; c) D. Sun, A. E. Riley, A. J. Cadby, E. K. Richman, S. D. Korlann, S. H. Tolbert, *Nature* **2006**, *441*, 1126–1130.
[31] M. M. Bentlohner, M. Waibel, P. Zeller, K. Sarkar, P. Müller-Buschbaum, D. Fattakhova-Rohlfing, T. F. Fässler, *Angew. Chem.* **2016**, *128*, 2487-2491; *Angew. Chem. Int. Ed.* **2016**, *55*, 2441-2445.
[32] a) R. A. Bley, S. M. Kauzlarich, *J. Am. Chem. Soc.* **1996**, *118*, 12461-12462; b) D. Neiner, H. W. Chiu, S. M. Kauzlarich, *J. Am. Chem. Soc.* **2006**, *128*, 11016-11017; c) B. R. Taylor, S. M. Kauzlarich, H. W. H. Lee, G. R. Delgado, *Chem. Mater.* **1998**, *10*, 22-24; d) B. M. Nolan, T. Henneberger, M. Waibel, T. F. Fässler, S. M. Kauzlarich, *Inorg. Chem.* **2015**, *54*, 396-401.
[33] D. Neiner, S. M. Kauzlarich, *Chem. Mater.* **2010**, *22*, 487-493.
[34] D. Mayeri, B. L. Phillips, M. P. Augustine, S. M. Kauzlarich, *Chem. Mater.* **2001**, *13*, 765-770.
[35] S. Scharfe, F. Kraus, S. Stegmaier, A. Schier, T. F. Fässler, *Angew. Chem.* **2011**, *123*, 3712–3754; *Angew. Chem. Int. Ed.* **2011**, *50*, 3630-3670.
[36] M. Waibel, O. Pecher, B. Mausolf, F. Haarmann, T. F. Fässler, *Eur. J. Inorg. Chem.* **2013**, *2013*, 5541-5546.
[37] F. Haarmann, in *eMagRes* (Eds.: R. K. Harris, R. E. Wasylishen), John Wiley & Sons, Ltd, Chichester, **2011.**
[38] O. Pecher, B. Mausolf, K. Lamberts, D. Oligschläger, C. Niewieszol (née Merkens), U. Englert, F. Haarmann, *Chemistry – A European Journal* **2015**, *21*, 13971-13982.
[39] J. Witte, H. G. von Schnering, W. Klemm, *Z. Anorg. Allg. Chem.* **1964**, *327*, 260–273.
[40] Free refinement of the site occupancy factors for all K positions from the single crystal X-ray diffraction experiment shows full occupation for all three sites.
[41] L. Vegard, *Z. Physik* **1921**, *5*, 17-26.
[42] T. Goebel, Dissertation, Technische Universität Dresden **2011**.
[43] The Na and Na4Si4 impurities cannot be detected in the respective powder diffraction pattern and must therefore be minute. The main reflections of K_3NaSi_4 are barely visible in the powder diffraction pattern and could not be reasonably included into the Rietveld refinement.
[44] O. Pecher, P. M. Bayley, H. Liu, Z. Liu, N. M. Trease, C. P. Grey, *J. Magn. Reson.* **2016**, *265*, 200-209.
[45] *APEX Suite of Crystallographic Software*, Bruker AXS Inc., Madison, WI, USA, **2008**.
[46] *SAINT*, Bruker AXS Inc., Madison, WI, USA, **2001**.
[47] *SADABS*, Bruker AXS Inc., Madison, Wisconsin, USA, **2001**.
[48] G. M. Sheldrick, *Acta Crystallogr. Sect. A* **2008**, *64*, 112–122.
[49] V. Petříček, M. Dušek, L. Palatinus, *Z. Kristallogr. - Cryst. Mater.* **2014**, *229*, 345.
[50] a) R. K. Harris, E. D. Becker, *J. Magn. Reson.* **2002**, *156*, 323-326; b) R. K. Harris, E. D. Becker, S. M. C. De Menezes, P. Granger, R. E. Hoffman, K. W. Zilm, *Magn. Reson. Chem.* **2008**, *46*, 582-598; c) R. K. Harris, E. D. Becker, S. M. Cabral de Menezes, R. Goodfellow, P. Granger, *Magn. Reson. Chem.* **2002**, *40*, 489-505.
[51] a) C. J. Pickard, F. Mauri, *Phys. Rev. B* **2001**, *63*, 245101; b) J. R. Yates, C. J. Pickard, F. Mauri, *Phys. Rev. B* **2007**, *76*, 024401; c) M. Profeta, F. Mauri, C. J. Pickard, *J. Am. Chem. Soc.* **2003**, *125*, 541-548.
[52] S. J. Clark, M. D. Segall, C. J. Pickard, P. J. Hasnip, M. I. J. Probert, K. Refson, M. C. Payne, *Z. Kristallogr.* **2005**, *220*, 567.
[53] J. P. Perdew, K. Burke, M. Ernzerhof, *Phys. Rev. Lett.* **1996**, *77*, 3865-3868.
[54] H. J. Monkhorst, J. D. Pack, *Phys. Rev. B* **1976**, *13*, 5188-5192.

Entry for the Table of Contents

FULL PAPER

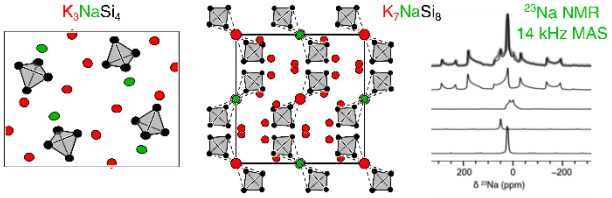

New Zintl Phases. $K_{4-x}Na_xSi_4$ ($1 \le x \le 2.2$) and K_7NaSi_8 are the first two ternary phases in the K-Na-Si system. The compounds both contain tetrahedral $[Si_4]^{4-}$ clusters which are isolated in $K_{4-x}Na_xSi_4$ and connected to linear $[Na(Si_4)_2]^{7-}$ dimers in K_7NaSi_8 (s. Figure). Solid-state NMR studies coupled with QM calculations show the anisotropic chemical bonding in K_7NaSi_8.

*Lavinia M. Scherf, Oliver Pecher, Kent J. Griffith, Frank Haarmann, Clare P. Grey, and Thomas F. Fässler**

Page No. – Page No.

The Ternary Zintl Phases $K_{4-x}Na_xSi_4$ ($1 \le x \le 2.2$) and K_7NaSi_8 – Synthesis, Crystal Structure, and Chemical Bonding